Journal of Non-Crystalline Solids 620 (2023) 122597

Contents lists available at ScienceDirect

Journal of Non-Crystalline Solids

journal homepage: www.elsevier.com/locate/jnoncrysol

Prediction of the surface chemistry of calcium aluminosilicate glasses

S. Miri Ramsheh [a], M. Turchi [a,f], S. Perera [b], A.M. Schade [c], D.V. Okhrimenko [d], S.L.S. Stipp [e], M. Solvang [d], T.R. Walsh [b], M.P. Andersson [a,*]

[a] Department of Chemical and Biochemical Engineering, Technical University of Denmark, Lyngby Kgs 2800, Denmark
[b] Institute for Frontier Materials, Deakin University, Geelong, VIC 3216, Australia
[c] Department of Chemistry and Bioscience, Aalborg University, Aalborg Ø 9220, Denmark
[d] ROCKWOOL A/S, Hedehusene 2640, Denmark
[e] Department of Physics, Technical University of Denmark, Lyngby, Kgs 2800, Denmark
[f] Laboratory of Multiscale Studies in Building Physics, Dübendorf, EMPA 8600, Switzerland

ARTICLE INFO

Keywords:
Density functional theory
Molecular dynamics
COSMO-RS
pK_a prediction
Dissolution

ABSTRACT

We have used a combination of density functional theory, the implicit solvent model COSMO-RS and molecular dynamics simulations to predict the pK_a of surface groups on calcium aluminosilicate glasses. We found that the average of pK_a for deprotonation and protonation for silanols agrees well with the point of zero charge for pure silica materials. Similarly, the average of pK_a for deprotonation and protonation for aluminols agrees well with the point of zero charge for pure alumina. We identified trends in the pK_a related to the hydrogen bonding of the surface groups, as well as the influence of tri-briding oxygen defects.

1. Introduction

Stone wool is a material widely used as sound and building insulation and for a range of industrial applications [1]. It is a material that consists of amorphous inorganic fibers which are mainly composed of oxides of silicon (SiO_2), aluminum (Al_2O_3), calcium (CaO), magnesium (MgO) and iron (Fe_2O_3), along with minor amounts of sodium, potassium and titanium [2]. Knowing the rates of stone wool dissolution in fluids is important from two perspectives. First, for health and safety during production and installation, stone wool should have a low bio-persistence (high dissolution rate) in lung fluids [3–9]. Second, the resistance of stone wool to weathering in contact with water, air and oxygen should be high enough for an economically reasonable durability for the desired use and low ecotoxicological effects [10]. For stone wool, the dissolution rate has been shown to be dependent on material [11–14] as well as solution composition [14,15], including pH, organic compounds present in the solution and temperature.

The surface chemistry of aluminosilicate glass is expected to play a key role in the mechanisms of the dissolution, including direct pH dependent dissolution and adsorption properties of key solution enhancers, such as citric acid [16,17]. Understanding how the surface chemistry in different conditions correlates with dissolution rate at those conditions could help identify key aspects of the dissolution mechanisms. In this study, we aimed at mapping the surface behavior of calcium aluminosilicate (**Ca**O-**Al**$_2$O$_3$-**Si**O$_2$, CAS) glasses using computational chemistry in the form of quantum chemistry. Earlier related work on silanol and aluminol proton affinities include Refs. [18,19]. CAS surfaces have also more recently been studied using molecular dynamics, including *ab initio* molecular dynamics[20] and reactive force fields [21–23]. CAS consists of the major network formers (Al and Si) and a common network modifier (Ca) and has often been used as a model for other kinds of amorphous materials, like stone wool, thanks to the simple composition (e.g. Refs. [24–26]).

Here, we employed density functional theory (DFT) combined with the COSMO-RS implicit solvent model to determine the protonation and deprotonation behavior of hydroxyl groups and water associated with cations in the solid, via prediction of the pK_a. The pK_a of the surface groups allows an understanding of how the surface chemistry and surface charge will change as a function of changing pH:

- For the surface reaction $Si\text{-}OH^{2+} \rightleftharpoons Si\text{-}OH$, if $pH < pK_a$ the protonated silanol dominates.
- For the surface reaction $Si\text{-}OH \rightleftharpoons Si\text{-}O^{-}$, if $pH > pK_a$, the deprotonated silanol dominates.

The pH dependent surface chemistry of other inorganic materials has

* Corresponding author.
E-mail address: martan@kt.dtu.dk (M.P. Andersson).

https://doi.org/10.1016/j.jnoncrysol.2023.122597
Received 7 June 2023; Received in revised form 17 July 2023; Accepted 21 August 2023
Available online 31 August 2023

previously been investigated using computational methods, including COSMO-RS for calcite [27,28] and *ab initio* molecular dynamics simulations for goethite [29]. The trends in pK_a for the surface groups on CAS would immediately provide key insights into pH and composition dependent surface chemistry and are likely related to the dissolution behavior. It also acts as a reference for experimental surface charge measurements and further studies with additives. The surface affinity for organic compounds as additives is expected to be dominated by the charge relationships between the surface and the functional group that attaches.

2. Computational methods

To produce the bulk structure of aluminosilicates as a reference for our work, we used the same procedure as in a recent study [30], which employed molecular dynamics (MD) simulations to predict bulk structure of calcium aluminosilicates with different compositions, namely, CAS1, CAS2, CAS3 and anorthite. The results were consistent with experimental data [30]. The compositions of the solids are shown in Table 1. From the bulk structure, smaller clusters with the same stoichiometry as the bulk were constructed and finally free energy calculations using DFT and the COSMO-RS implicit solvent model were used to obtain the pK_a for the surface groups of these clusters. We chose a cluster model because pK_a prediction using COSMO-RS is unavailable in periodic boundary conditions. Our chosen size of clusters also allowed for fast calculations, which allowed us to model several clusters and many different surface sites. We assumed that this procedure would provide a more complete probe of the various amorphous local surface structures available. The procedures for creating the spheres and the following DFT calculations are now described in more detail.

2.1. Molecular dynamics simulations

In this work, all MD simulations were performed with the LAMMPS software [31] (http://lammps.sandia.gov) . MD simulations were used in two different stages:

Self-forming of the CAS sphere interface in vacuum. For each of the CAS glasses, the bulk structures were initially set up by inserting randomly positioned atoms within a simulation periodic cell. The composition of the CAS structures, together with the initial number of atoms for each of the bulk and sphere structures, are reported in Table 1. At this stage, the recently developed (Sundararaman, Huang, Ipsas, Kob) SHIK potential [24] was employed. After an energy minimization step with the conjugate gradient method, the system was subsequently heated to 3500 K and equilibrated for 500 ps in the NVT ensemble. For each composition, the so-formed melted structures were cooled to 2000 K in the NVT ensemble at a quench rate of 2.25 K/ps using a timestep of 1 fs. At this point, a sphere was cut from the bulk using an in-house code, which for a given center and radius of the sphere, is able to identify the correct stoichiometry of the CAS structure. The code only retains structures which match the bulk material stoichiometry (Fig. 1). Finally, each of the cut spheres was quenched from 2000 K to 300 K in vacuum, thus allowing the interface to form itself.

Solvation of the CAS sphere in water. Each sphere that was extracted in the first stage was transferred to a smaller simulation cell with dimensions 22 Å x 22 Å x 22 Å and subsequently water molecules were inserted around the sphere to solvate the structure. Using the PACKMOL software[32], 300 water molecules were added around each of the sphere in order to match the density of bulk water. The solvated CAS structures were subsequently simulated using the reactive ReaxFF force field [33,34] as implemented in LAMMPS [34]. The parameters ware taken from Refs. [35,36] except for Ca, which were taken from Ref. [37]. After an energy minimization step employing the conjugate gradient method, the simulation was run in the NVT ensemble for 0.5 ns, at a constant temperature of 300 K, and in the NPT ensemble for 0.5 ns, at constant temperature of 300 K and a pressure of 1 bar, using a timestep of 0.25 fs. Previous work reported a time of about 1 ns to allow for water molecules to react with a quartz interface [38,39]. The only goal of the ReaxFF simulations was to hydroxylate the cluster surface and at the end of our simulation, some hydroxyl groups at the spheres/water interface were observed. We used an in-house script to identify the hydroxyls and water coordinated with Ca^{2+}, Al^{3+} and Si^{4+} on the sphere surface. In this way, each of the hydrated/hydroxylated spheres (characterized by radii of around 15 Å and containing around 150 atoms, including the solvation water shell) were extracted from the simulation cell and subsequently subjected to a semi-empirical optimization step (see next section) before the DFT calculations.

There are three kinds of surface groups relevant to our study, each associated with a certain cation; aluminols (>Al-OH), silanols (>Si-OH) and Ca^{2+} hydration waters (Ca-$(H_2O)^{2+}$). These are shown in Fig. 2.

The spheres surfaces are dominated by Ca^{2+} ions with their hydration water molecules. Therefore, to improve the statistics for aluminol and silanol surface chemistry, we also modified the clusters by removing the Ca^{2+} ions on the surface to generate a model for the surface that is dominated by the network forming ions Si^{4+} and Al^{3+}. This mimics results from CAS dissolution experiments, where Ca^{2+} ions is often leached, significantly faster than the network formers [40,41]. It is therefore possible that hydrolysis of the network bonds is the rate limiting step of dissolution and the chemistry of aluminol and silanol becomes particularly important. The pK_a of the network former surface groups aluminol and silanol (Fig. 2) presented later includes data from the original clusters as well as clusters where the Ca^{2+} was removed.

2.2. Semi-empirical optimization and DFT calculations

The structures of all the solvated spheres that we extracted from the MD simulations had difficulties converging directly with DFT calculations. Therefore, we made a semi-empirical energy minimization step, prior to the DFT calculations. This intermediate step was applied only to the charge-neutral spheres. Once the structure of each charge-neutral sphere was energy-minimized in this way, the relative deprotonated structures were calculated solely with DFT, based on the structure of each corresponding neutral sphere optimized geometry. We used MOPAC [42], a general-purpose semiempirical molecular orbital package, to do the semiempirical energy minimization on the solvated spheres from the MD simulations. We fixed the position of all hydrogen and oxygen atoms and used the PM7 method for energy minimization by optimizing the configurations for calcium, aluminum and silicon ions. This partial optimization was enough to allow all following DFT calculations to converge smoothly and maintain the amorphous structure from the MD simulations. The partial freezing was done to keep the cluster structure as close to the MD generated structure as possible before the DFT optimization.

All the DFT calculations were performed with the Turbomole software, v 7.4.0 [43]. Full geometry optimizations were carried out using a Becke-Perdew (BP) functional [44,45], the TZVP basis set [46], the resolution of identity (RI) approximation together with the COSMO [47] implicit solvent model and an infinite dielectric constant (needed for subsequent COSMO-RS calculations [48]). By means of DFT calculations, the molecular screening charge surface, also known as σ-surface or COSMO surface in COSMO-RS theory, was computed for all the neutral, deprotonated and protonated CAS spheres (such as Fig. 3). The

Table 1
Composition and total number of atoms for the four compositions for the bulk glass simulations.

Compositions	CaO%mol	Al_2O_3%mol	SiO_2%mol	no. of atoms
CAS1	43.5	13.0	43.5	9750
CAS2	42.5	15.0	42.5	10,800
CAS3	40.0	20.0	40.0	10,800
Anorthite	25.0	25.0	50.0	9360

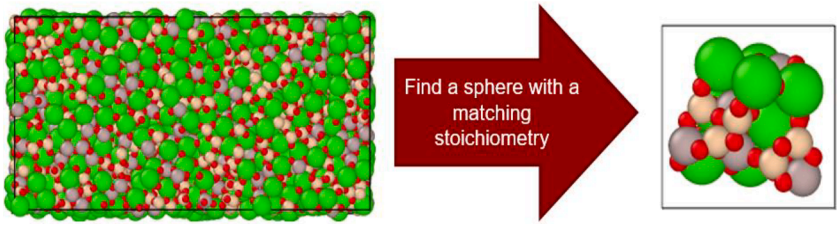

Fig. 1. – Cutting a spherical structure from the bulk with a matching stoichiometry.

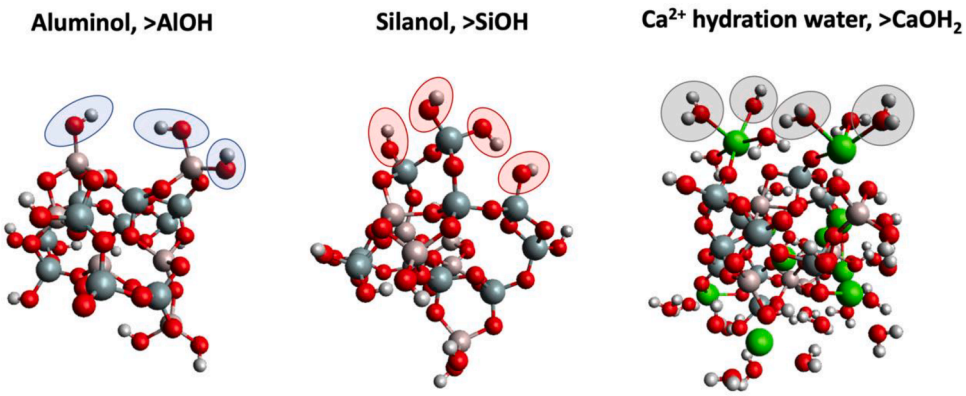

Fig. 2. Illustration of the three kinds of surface groups on CAS we studied for (de)protonation. The aluminols and silanols are shown on clusters with surface Ca^{2+} ions removed. All kinds of groups are present on the clusters, but they are simply rotated to show the desired kind of group towards the top for each case. Color code: H=white, O=red, Al=light purple, Si=grey, Ca=green.

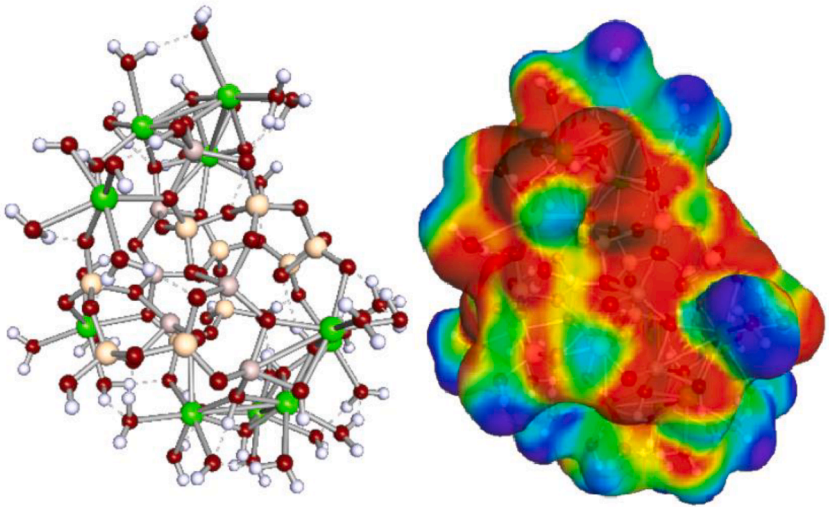

Fig. 3. Molecular structure and COSMO surface of a CAS1 sphere after geometry optimization with Turbomole.

information for the σ-surface of each sphere (neutral and deprotonated) is stored in the .cosmo files.

The actual pK_a predictions were performed using COSMO-RS as implemented in the COSMOtherm software, and are based on a linear free energy relationship (LFER) between measured pK_a and the calculated free energy difference between the protonated and the deprotonated spheres [49]. The LFER therefore only requires input via the .cosmo files of the charge-neutral and the relative deprotonated spheres or via the protonated sphere and the charge-neutral one, where the charge-neutral state is defined as a hydroxyl for >Si-OH and >Al-OH and defined as water for $>Ca(H_2O)_x^{2+}$. It is thus not defined by the overall charge of the cluster. As an indication for the reliability of our chosen method, we predicted the pK_a for the silicic acid monomer to be 8.1, which is in reasonable agreement with the experimental value of 9.5 [50], although slightly underestimated.

3. Results and discussion

3.1. pK_a predictions

To analyze the predicted pK_a, we classified them by the nature of the deprotonated hydrogen site on the surface of the sphere. Table 2 presents a description, the number of pK_a, as well as the average and standard deviation for each pK_a class. For a classification to make sense, we looked for chemical bonding similarities (especially hydrogen bonds with adjacent surface groups) which exhibited a narrow distribution.

Table 2
Classification of silanol and aluminol hydroxyl groups on aluminosilicate surface and their corresponding pK_a. HB = hydrogen bond, HBD = Hydrogen bond donor, HBA = Hydrogen Bond Acceptor, TBO = three bridging oxygen. > indicates a surface bound group and is not an indication of the number of network bonds.

	Type	Description	Number of cases	Average pK_a	Standard Deviation
>Si-OH	S1	Si(OH) or $Si(OH)_2$, no HB, / HBD to Al-OH or Si-OH	30	7.3	1.3
	S2	Si(OH) or $Si(OH)_2$, HBD to a bridging O	6	10.4	1.4
	S3	Si(OH) or $Si(OH)_2$, HBA/ Si $(OH)_3$	6	3.3	0.9
	S4	Si(OH) or $Si(OH)_2$, bonded to TBO	5	4.9	0.5
>Si-OH		**Average**	**47**	**6.9**	**2.2**
$>Si\text{-}OH_2^+$	S5	$Si\text{-}OH_2^+$, not bonded to TBO	29	−6.0	2.4
	S6	$Si\text{-}OH_2^+$, bonded to TBO	4	−8.0	3.5
$>Si\text{-}OH_2^+$		**Average**	**33**	**−6.2**	**2.5**
>Al-OH	A1	Al(OH) or Al(OH)2, no HB,	16	16.7	0.8
	A2	$Al(OH)_2$ or $Al(OH)_3$, HBD to Al-OH or Si-OH / Al(OH) or Al $(OH)_2$ bonded to TBO	8	11.1	1.1
	A3	$Al(OH)_3$, HBA	1	7.0	–
>Al-OH		**Average (excluding A3)**	**24**	**14.8**	**1.0**
$>Al\text{-}OH_2^+$	A4	$Al\text{-}OH_2^+$, normal	10	2.1	1.6
	A5	$Al\text{-}OH_2^+$, bonded to TBO	12	−0.2	1.8
$>Al\text{-}OH_2^+$		**Average**	**22**	**0.8**	**1.7**
Ca-H_2O	C	Ca-H_2O	145	9.2	1.9

For all the classifications in Table 2 (except protonation of silanols (S5, S6)), the standard deviation was below 2 pH units. The number of cases in each group is a measure of the prevalence of that kind of group on the surface, so it can be used to predict the relative proportion of each type, with a caveat. The clusters are significantly smaller than a real surface (i.e. much higher curvature), so we expect these relative proportions to be qualitative rather than quantitative.

For all the clusters, we also predicted the pK_a for protonation of the bridging oxygens. Because of the amorphous nature of the material, the clusters are only metastable. Therefore, there could be an unwanted relaxation of the covalent network geometry during protonation and deprotonation. To make sure that we did not experience undesired relaxation of the network structure, we used these bridging oxygen pK_a predictions to test the stability of the covalent network by deprotonating the stable protonated structures back to the unprotonated oxygen bridge. For a "normal" molecule, the identical deprotonated state was found, but for complex amorphous structures in a metastable state, this was not necessarily the case. For some of our clusters, we found a difference of more than 1 pH unit. These results were excluded from the study, because there is no way to distinguish the free energy change coming from (de)protonation or additional structure relaxation. The pK_a that were resilient to the consequent deprotonation are presented in Table 3. All pK_a in Table 2 are also only from the same resilient clusters.

The protonation of silanol had so low pK_a (Table 2) that we chose not to present them in Fig. 3. However, the values are reasonable despite being so low, when considered together with the deprotonation pK_a. The average of protonation and deprotonation pK_a should theoretically be equal to the point of zero charge. This average of the average pK_a for the silanols, is 0.7, which is consistent with the point of zero charge for silica, which is typically $\lesssim 2$ [51]. The average of protonation and deprotonation of "normal" aluminol groups A1 and A4, is 9.4, which is close to the point of zero charge for alumina, which is typically ~9 [51]. This indicates that our results are reasonable, that the local chemistry of the (de)protonating group is the main driver for the pK_a and that the chemistry of aluminol and silanol groups is similar across a range of materials. Additional calculations for more materials would be necessary to confirm this suggestion. Considering the underestimation of the point of zero charge for the silanols and the similar underestimate of the silicic acid pK_a, it could be assumed that our silanol deprotonation pK_a are systematically underestimated by 1–2 pH units. For the bridging oxygens, the composition of the cations making up the bridge with the oxygen defined the pK_a. Al-O-Al bridges had a rather high pK_a of 3.1, which could mean a significant amount of protonation within the normal pH range. This is particularly interesting for the sake of biosolubility, which is generally analyzed at pH 4.5, which is quite close to the pK_a of 3.1. The pK_a of Si-O-Si bridges is low, −5.3, which is similar in value to the protonation of silanol groups and lower than the pK_a of hydronium ions, −1.7. Periodic density functional theory calculations of a silica-water interface [19] found that Si-(OH^+)-Si bridges were unstable compared to either $>SiOH_2^+$ or adsorbed H_3O^+. Our results are consistent with the study [19] in that our silanol and Si-O-Si protonation pK_a is lower than the pK_a of the hydronium ion. They differ in that our silanol and Si-O-Si bridge pK_a are similar. If the underestimation of silanol pK_a are not applicable to bridging Si-O-Si protonation, there is qualitative agreement, but we don't have enough data to make that call.

Fig. 4 shows the predicted pK_a values for (a) protonation and deprotonation of aluminol, (b) deprotonation of silanol and (c) deprotonation of hydration waters associated with calcium ions.

Aluminol: The pK_a values for aluminol groups, including both protonation and deprotonation, are categorized into five types (A1 through A5 in Fig. 3(a)), varying widely from −2 to 19. Type A1 includes >Al-OH and >Al-$(OH)_2$ groups which have no H-bond, are tetrahedrally coordinated and have pK_a values between 15 and 19. The second Type (A2) is the combination of two kinds of aluminols, either >Al-$(OH)_2$/>Al-$(OH)_3$ groups which donate a hydrogen bond to another >Al-OH/>Si-OH on the surface or >Al-OH/>Al$(OH)_2$ groups having the aluminum atom bonded to a three bridging oxygen (TBO). The pK_a values of Type A2 fall in the range of 9–14 with an average value that is 5.6 units lower than the one of Type A1. Type A3 includes only one case, *a* >Al-$(OH)_3$ group being a hydrogen bond acceptor, with a pK_a value of 7.0. This will not be discussed further in this work, based on the lack of statistics. Type A4, including $>Al\text{-}OH_2^+$ groups where aluminum is tetrahedrally coordinated on the surface, have pK_a ranging from −1 to 5, with an average of 2.1. Type A5 includes $>Al\text{-}OH_2^+$ groups but with an aluminum that is bonded with a TBO; pK_a for this type ranges between −2 and 4 with an average of −0.2 (2.3 units lower than for A4). The similarity in chemical environment means that classes A1 and A4 could be considered pK_{a1} and pK_{a2} for "normal" aluminol groups and A2 and A5 could be considered pK_{a1} and pK_{a2} for aluminols bonded to TBO defects.

Silanol: For silanol deprotonation, we have classified our observations into four types (S1 through S4 in Fig. 3(b)). Type S1 includes a combination of two, >Si(OH)/>Si$(OH)_2$ groups with no hydrogen bonding and the silicon tetrahedrally coordinated, and the ones that are

Table 3
pK_a for protonation of bridging oxygen as a function of the atomic nature of the bridge.

Linkage	Number of cases	Average pK_a	Standard deviation
Si-O-Si	4	−5.3	2.1
Si-O-Al	13	−2.4	2.2
Al-O-Al	3	3.1	1.0

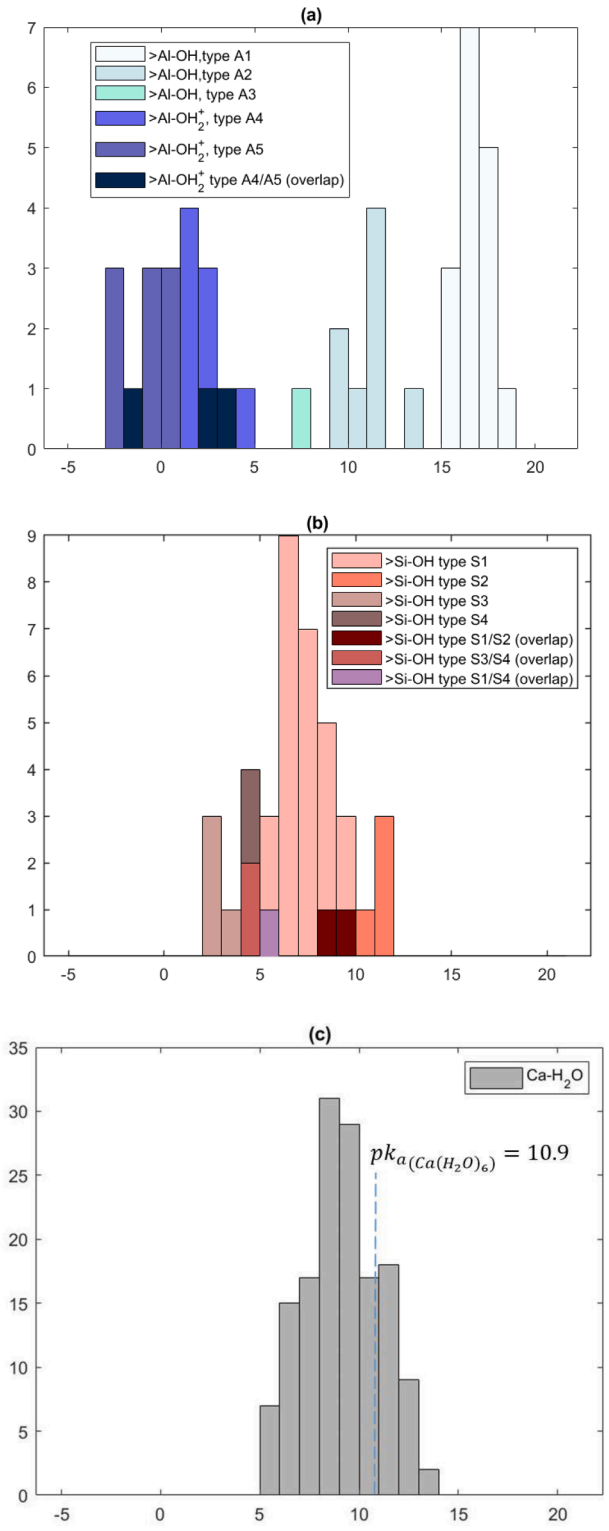

Fig. 4. COSMO-RS predicted pK_a of (a) aluminol (b) silanol (c) hydration water at the surface associated with Ca^{2+} on amorphous CAS material (CAS1, CAS2, CAS3 and anorthite).

H-bond donors to >Si-OH or >Al-OH . Type S1 pK_a range from 5.0 to 10.0 with an average of 7.3. Type S2 comprises >Si(OH)/>Si$(OH)_2$ which are hydrogen bond donors to a bridging oxygen. The predicted values of pK_a for Type S2 range from 8 to 12 with an average value of 10.4, 3.1 units higher than Type S1. Type S3 also has two different structures having similar pK_a values; >Si(OH)/Si$(OH)_2$ groups which are hydrogen bond acceptors, and Si$(OH)_3$ groups. Type S3 is characterized by pK_a values ranging from 2.0 to 5.0 with an average of 3.3, 4.0 units lower than for Type S1. Finally, Type S4 consists of >Si(OH)/Si$(OH)_2$ with Si bonded to a TBO, for which pK_a spans between 4 and 6, with an average of 4.9. The stronger overlap in the pK_a classifications for silanol groups (i.e. smaller difference between average pK_a values) as compared to aluminol suggests that it would be possible to represent silanol deprotonation using a single pK_a with a wider spread. The average pK_a is 6.9 if all silanol deprotonations are treated as a single group (Table 2).

Silanol vs aluminol behavior: When comparing the results for silanols and aluminols, we get the trend $pK_{a1,SiOH} < pK_{a1,AlOH} < pK_{a2,SiOH} < pK_{a2,AlOH}$, where the subscript 1 is protonation and 2 is deprotonation. This trend in pK_a is consistent with relative values of proton affinities for small silanol and aluminol models[18] It is also consistent with reactive force field modeling of a CAS-water interface [23], which found >Al-OH_2^+ surface groups forming during the simulation, but no >Si-OH_2^+ groups. Some of our pKa for aluminol protonation are as high as 5, which means that for some surface group configurations, >Al-OH_2^+ groups could form spontaneously during a well-parameterized MD simulation for reasonable pH conditions. The silanol protonation pK_a are far too low for protonated groups to be expected to form.

Hydrated calcium: Fig. 3(c) is a histogram of the predicted pK_a for hydration water molecules associated with calcium ions. pK_a ranges from 4 to 14 with an average value of 9.2. The pK_a distribution is quite coherent and reminiscent of a normal distribution. The average pK_a is 1–2 pH units lower than the corresponding hydrolysis constant in aqueous solution, also calculated with the same method, to keep the comparison consistent. This means that Ca at the surface does make the hydration water slightly more acidic than when it is attached to an ion that is free in solution. The amorphous structure of the solid impacts Ca hydration water, which is apparent from the distribution of pK_a where the standard deviation is 2 pH units.

Effect of hydrogen bonds: The trends in the pK_a averages listed in Table 1 show a clear relationship to the presence of hydrogen bonds with other surface groups. For >Al-OH deprotonation, being a hydrogen bond donor to an adjacent >Si-OH or >Al-OH group, the pK_a decreases by about 6 units. When >Al-OH acts as an H-bond acceptor, the pK_a decreases by almost 9 units, although at least some of the effect could result from it being a Q_1 group. The lack of statistics for these groups precludes drawing further conclusions, but we report it nonetheless for completeness. For >Si-OH deprotonation, we observed two types of H-bond influence on pK_a. Deprotonation from hydroxyl groups that are H-bond donors to bridging oxygen have an average pK_a about 3 units higher than those that do not participate in any H-bond. However, being an H-bond donor to >Al-OH or >Si-OH groups does not have a significant effect on pK_a. Also, >Si-OH that are H-bond acceptors have a significantly lower pK_a than those not involved in any H-bonds by 4.0 pH units.

Three bridging oxygen (TBO): The normal coordination number of oxygen with respect to Al or Si atoms is 2 (in the corresponding tetrahedral coordination for Si and Al). However, a very well-known defect in CAS systems, which has been reported in several MD simulation studies [26,52], is O atoms coordinated to 3 network formers (Si, Al or both); namely three bridging oxygen (TBO). Our results show that for aluminols (>Al$(OH)_x$ groups) and silanols (>Si$(OH)_x$ groups) where the network former is bonded with a TBO, pK_a is lower than those coordinated only with normal bridging oxygens. For silanols bonding with a TBO, pK_a is 2.4 units lower on average. This effect is even more dramatic for deprotonation of >Al(OH) for which pK_a is around 6 units lower.

pK_a correlation with neighbouring network formers

To investigate how the local environment could affect the protonation behavior, we tried to group the pK_a values based on which network formers their silanol or aluminol was linked to. We found that all groups, for either silanol or aluminol, have similar averages and large standard

deviations, indicating no correlation between the local environment and pK_a values.

pK_a correlations with Al-O and Si-O bond distances

Some studies (e.g. [53]), have reported a correlation between pK_a and bond distance, allowing for reasonable estimates of pK_a, for example from MD simulations, saving time compared with more time-consuming calculations, such as with the COSMO-RS method used here. For the CAS systems that we investigated, we did not find any general correlation, suggesting that full pK_a calculations are necessary, at least for the cluster models such as the ones that we have used. The details are shown in the Supporting Information.

4. Conclusions

We predicted the pK_a of surface groups on calcium aluminosilicate (CAS) glasses combining molecular dynamics simulations and density functional theory. The resulting average of pK_a for protonation and deprotonation of silanol groups is 0.7, which is consistent with the point of zero charge for silica. The resulting average of pK_a for protonation and deprotonation of aluminol groups is 9.4, which is consistent with the point of zero charge for alumina. Our results therefore seem reasonable. In contrast to crystalline materials, the amorphous materials studied here give rise to a distribution of pK_a rather than a single value. This distribution of pK_a is expected to impact how the surface charge varies as a function of pH, where an amorphous material is expected to have a weaker pH dependency for the charge.

We also identified some trends in the pK_a related to the chemical environment. In particular, we found that the pK_a was influenced by the presence of three bridging oxygen defects adjacent to the surface group or if the surface group was involved in hydrogen bonding to adjacent oxygen or hydroxyl groups. We expect the surface charge and surface chemistry to impact the dissolution rates of CAS materials, because it has been indicated in calculations that the hydrolysis barrier for silica dissolution is significantly different for neutral vs deprotonated and protonated surface silanol groups [54].

Declaration of Competing Interest

The authors declare the following financial interests/personal relationships which may be considered as potential competing interests:

The authors declare following competing financial interest(s): D.V.O and M.S are employees of ROCKWOOL A/S, a company producing stone wool fibers.

Data availability

No data was used for the research described in the article.

Acknowledgements

The authors gratefully acknowledge ROCKWOOL A/S for support of this research.

Supplementary materials

Supplementary material associated with this article can be found, in the online version, at doi:10.1016/j.jnoncrysol.2023.122597.

References

[1] A.M. Papadopoulos, State of the art in thermal insulation materials and aims for future developments, Energy Build 37 (2005) 77–86.
[2] Q. Zu, M. Solvang, H Li, H. Li, Commercial glass fibers. Fiberglass Science and Technology: Chemistry, Characterization, Processing, Modeling, Application, and Sustainability, Springer, 2021, pp. 1–89, https://doi.org/10.1007/978-3-030-72200-5.
[3] M. Guldberg, S.L. Jensen, T. Knudsen, T. Steenberg, O. Kamstrup, High-alumina low-silica HT stone wool fibers: a chemical compositional range with high biosolubility, Regul. Toxicol. Pharmacol. 35 (2002) 217–226.
[4] J.M.G Davis, Experimental studies on mineral fibre carcinogenesis: an overview, Mech. Fibre Carcinog. (1991) 51–58, https://doi.org/10.1007/978-1-4684-1363-2_6.
[5] A.W. Ng, A. Bidani, T.A. Heming, Innate host defense of the lung: effects of lung-lining fluid pH, Lung 182 (2004) 297–317. *2004 1825*.
[6] D.M. Bernstein, Synthetic vitreous fibers: a review toxicology, Epidemiol. Regul. 37 (2008) 839–886. 10.1080/10408440701524592.
[7] P. Harrison, et al., Regulatory risk assessment approaches for synthetic mineral fibres, Regul. Toxicol. Pharmacol. 73 (2015) 425–441.
[8] L.D. Maxim, J.G. Hadley, R.M. Potter, R Niebo, The role of fiber durability/biopersistence of silica-based synthetic vitreous fibers and their influence on toxicology, Regul. Toxicol. Pharmacol. 46 (2006) 42–62.
[9] O. Kamstrup, J.M.G. Davis, A. Ellehauge, M Guldberg, The biopersistence and pathogenicity of man-made vitreous fibres after short- and long-term inhalation, Ann. Occup. Hyg. 42 (1998) 191–199.
[10] E. Smollich, et al., Assessment of acute and chronic ecotoxicological effects of aqueous eluates of stone wool insulation materials, Environ. Sci. Eur. 35 (2023) 1–16.
[11] M. Guldberg, A. De Meringo, O. Kamstrup, H. Furtak, C Rossiter, The development of glass and stone wool compositions with increased biosolubility, Regul. Toxicol. Pharmacol. 32 (2000) 184–189.
[12] Bellmann, B., Schaeffer, H.A. & Muhle, H. Impact of variations in the chemical composition of vitreous mineral fibers on biopersistence in rat lungs and consequences for regulation. 10.3109/08958378.2010.483771 22, 817–827 (2010).
[13] Eastes, W., Potter, R.M. & Hadley, J.G. Estimating *in vitro* glass fiber dissolution rate from composition. 10.1080/089583700196149 12, 269–280 (2008).
[14] V.R. Christensen, S.L. Jensen, M. Guldberg, O Kamstrup, Effect of chemical composition of man-made vitreous fibers on the rate of dissolution in vitro at different pHs, Environ. Health Perspect. 102 (1994) 83.
[15] T. Steenberg, H.K. Hjenner, S. Jensen, M. Guldberg, T. Knudsen, Dissolution behaviour of biosoluble HT stone wool fibres, Glas. Sci. Technol. (2001).
[16] S.H.Q. Barly, D.V. Okhrimenko, M. Solvang, Y. Yue, S.L.S Stipp, Dissolution of stone wool fibers with phenol-urea-formaldehyde binder in a synthetic lung fluid, Chem. Res. Toxicol. 32 (2019) 2398–2410.
[17] D.V. Okhrimenko, et al., The dissolution of stone wool fibers with sugar-based binder and oil in different synthetic lung fluids, Toxicol. Vitr. 78 (2022), 105270.
[18] J.D. Kubicki, G.A. Blake, S.E. Apitz, *Ab initio* calculations on aluminosilicate Q3 species: implications for atomic structures of mineral surfaces and dissolution mechanisms of feldspars, Am. Mineral. 81 (1996) 789–799.
[19] A.V. Bandura, J.D. Kubicki, J.O. Sofo, Periodic density functional theory study of water adsorption on the α-quartz (101) surface, J. Phys. Chem. C 115 (2011) 5756–5766.
[20] J.M. Rimsza, J. Du, *Ab initio* molecular dynamics simulations of the hydroxylation of nanoporous silica, J. Am. Ceram. Soc. 98 (2015) 3748–3757.
[21] T.S. Mahadevan, J. Du, Atomic and micro-structure features of nanoporous aluminosilicate glasses from reactive molecular dynamics simulations, J. Am. Ceram. Soc. 104 (2021) 229–242.
[22] J. Kalahe, et al., Temperature dependence of interfacial reactions of sodium aluminosilicate glasses from reactive molecular dynamics simulations, Appl. Surf. Sci. 619 (2023), 156780.
[23] J. Kalahe, et al., Composition effect on interfacial reactions of sodium aluminosilicate glasses in aqueous solution, J. Phys. Chem. B 127 (2023) 269–284.
[24] S. Sundararaman, L. Huang, S. Ispas, W Kob, New interaction potentials for alkali and alkaline-earth aluminosilicate glasses, J. Chem. Phys. 150 (2019), 154505.
[25] F. Bouyer, G. Geneste, S. Ispas, W. Kob, P Ganster, Water solubility in calcium aluminosilicate glasses investigated by first principles techniques, J. Solid State Chem. 183 (2010) 2786–2796.
[26] G. Agnello, et al., Bulk structures of silica-rich calcium aluminosilicate (CAS) glasses along the molar CaO/Al_2O_3= 1 join via molecular dynamics (MD) simulation, J. Non. Cryst. Solids 519 (2019), 119450.
[27] M.P. Andersson, S.L.S Stipp, How acidic is water on calcite? J. Phys. Chem. C 116 (2012) 18779–18787.
[28] M.P. Andersson, J.D. Rodriguez-Blanco, S.L.S Stipp, Is bicarbonate stable in and on the calcite surface? Geochim. Cosmochim. Acta 176 (2016) 198–205.
[29] K. Leung, L.J. Criscenti, Predicting the acidity constant of a goethite hydroxyl group from first principles, J. Phys. Condens. Matter 24 (2012).
[30] M. Turchi, et al., Predicted structures of calcium aluminosilicate glass as a model for stone wool fiber: effects of composition and interatomic potential, J. Non. Cryst. Solids 567 (2021), 120924.
[31] S. Plimpton, Fast parallel algorithms for short-range molecular dynamics, J. Comput. Phys. 117 (1995) 1–19.
[32] L. Martínez, R. Andrade, E.G. Birgin, J.M. Martínez, PACKMOL: a package for building initial configurations for molecular dynamics simulations, J. Comput. Chem. 30 (2009) 2157–2164.
[33] T.P. Senftle, et al., The ReaxFF reactive force-field: development, applications and future directions, NPJ Comput. Mater. 21 (2) (2016) 1–14. *2016*.
[34] A.C.T Van Duin, et al., ReaxFFSiO reactive force field for silicon and silicon oxide systems, J. Phys. Chem. A 107 (2003) 3803–3811.

[35] L. Liu, A. Jaramillo-Botero, W.A. Goddard, H Sun, Development of a ReaxFF reactive force field for ettringite and study of its mechanical failure modes from reactive dynamics simulations, J. Phys. Chem. A 116 (2012) 3918–3925.
[36] G.M. Psofogiannakis, J.F. McCleerey, E. Jaramillo, A.C.T. Van Duin, ReaxFF reactive molecular dynamics simulation of the hydration of Cu-SSZ-13 zeolite and the formation of Cu dimers, J. Phys. Chem. C 119 (2015) 6678–6686.
[37] H. Manzano, R.J.M. Pellenq, F.J. Ulm, M.J. Buehler, A.C.T. Van Duin, Hydration of calcium oxide surface predicted by reactive force field molecular dynamics, Langmuir 28 (2012) 4187–4197.
[38] J.C. Fogarty, H.M. Aktulga, A.Y. Grama, A.C.T. Van Duin, S.A Pandit, A reactive molecular dynamics simulation of the silica-water interface, J. Chem. Phys. 132 (2010), 174704.
[39] J.M. Rimsza, J. Yeon, A.C.T. Van Duin, J Du, Water interactions with nanoporous silica: comparison of reaxff and *ab initio* based molecular dynamics simulations, J. Phys. Chem. C 120 (2016) 24803–24816.
[40] D.V. Okhrimenko, et al., Surface evolution of aluminosilicate glass fibers during dissolution: influence of pH, solid-to-solution ratio and organic treatment, J. Colloid Interface Sci. 606 (2022), 1983–1997.
[41] D.V. Okhrimenko, et al., Surface reactivity and dissolution properties of alumina-silica glasses and fibers, ACS Appl. Mater. Interfaces 12 (2020) 36740–36754.
[42] J.J.P Stewart, MOPAC: a semiempirical molecular orbital program, J. Comput. Mol. Des. 41 (4) (1990) 1–103, 1990.
[43] R. Ahlrichs, M. Bär, M. Häser, H. Horn, C. Kölmel, Electronic structure calculations on workstation computers: the program system turbomole, Chem. Phys. Lett. 162 (1989) 165–169.
[44] A.D. Becke, Density-functional exchange-energy approximation with correct asymptotic behavior, Phys. Rev. A 38 (1988) 3098–3100.
[45] J.P. Perdew, Density-functional approximation for the correlation energy of the inhomogeneous electron gas, Phys. Rev. B Condens. Matter 33 (1986) 8822–8824.
[46] F. Weigend, R. Ahlrichs, Balanced basis sets of split valence, triple zeta valence and quadruple zeta valence quality for H to Rn: design and assessment of accuracy, Phys. Chem. Chem. Phys. 7 (2005) 3297–3305.
[47] A. Klamt, G. Schüürmann, COSMO - a new approach to dielectric screening in solvents with explicit expressions for the screening energy and its gradient, J. Chem. Soc. Perkin Trans. 2 Phys. Org. Chem. (1993) 799–805.
[48] A. Klamt, F. Eckert, W. Arlt, COSMO-RS: an alternative to simulation for calculating thermodynamic properties of liquid mixtures, Annu. Rev. Chem. Biomol. Eng. 1 (1) (2010) 101–122.
[49] A. Klamt, F. Eckert, M. Diedenhofen, M.E Beck, First principles calculations of aqueous pK(a) values for organic and inorganic acids using COSMO-RS reveal an inconsistency in the slope of the pK(a) scale, J. Phys. Chem. A 107 (2003) 9380–9386.
[50] J.D. Kubicki, Self-consistent reaction field calculations of aqueous Al_3+, Fe_3+, and Si_4+: calculated aqueous-phase deprotonation energies correlated with experimental Ln(Ka) and pKa, J. Phys. Chem. A 105 (2001) 8756–8762.
[51] M. Kosmulski, The pH dependent surface charging and points of zero charge. VIII. Update, Adv. Colloid Interface Sci. 275 (2020), 102064.
[52] A. Atila, E.M. Ghardi, A. Hasnaoui, S. Ouaskit, Alumina effect on the structure and properties of calcium aluminosilicate in the percalcic region: a molecular dynamics investigation, J. Non. Cryst. Solids 525 (2019), 119470.
[53] C. Dardonville, et al., Substituent effects on the basicity (pKa) of aryl guanidines and 2-(arylimino)imidazolidines: correlations of pH-metric and UV-metric values with predictions from gas-phase *ab initio* bond lengths, New J. Chem. 41 (2017) 11016–11028.
[54] S. Nangia, B.J Garrison, Reaction rates and dissolution mechanisms of quartz as a function of pH, J. Phys. Chem. A 112 (2008) 2027–2033.